Available online at www.sciencedirect.com
ScienceDirect
Journal of the European Ceramic Society 29 (2009) 1887–1894
www.elsevier.com/locate/jeurceramsoc

Preparation of double-layer glass-ceramic/ceramic tile from bauxite tailings and red mud

Huizhi Yang [a,*], Changping Chen [b], Lijun Pan [b], Hongxia Lu [b], Hongwei Sun [b], Xing Hu [b]

[a] *Department of Mathematical and Physical Sciences, Henan Institute of Engineering, Zhengzhou 451191, China*
[b] *School of Physical Engineering and Laboratory of Material Physics, Zhengzhou University, Zhengzhou 450052, China*

Received 1 April 2008; received in revised form 26 December 2008; accepted 7 January 2009
Available online 1 February 2009

Abstract

Double-layer glass-ceramic/ceramic tiles made from bauxite tailings and red mud were prepared using a single firing powder processing route. The influence of the preparation method used for the green bodies on the microstructure and mechanical properties of the final products was investigated. The macroscopic appearance, microstructure, and mechanical properties indicated that the production of double-layer glass-ceramic/ceramic tiles may be an attractive method for recycling industrial waste into building materials.

Keywords: Glass-ceramic; Waste; Tile

1. Introduction

The large amount of industrial waste, such as red mud (RM) from alumina production, tailings from the ore-dressing process and waste glass from bottle banks, has caused serious environmental problems. In recent years, more attention has been paid to recycling and safely treating these wastes in both developed and developing countries.[1–3] A promising way to reuse these wastes is to use them to produce building materials, such as porcelain tiles[4–12] and glass-ceramics.[13–21]

Although there are obvious environmental benefits to be gained from the recycling of wastes in producing glass-ceramics and porcelain tiles, some aspects limit their applications, as well as their commercial success. The production costs for glass-ceramics are higher than those for porcelain tiles, and impurities in the wastes (such as Fe_2O_3) often color the final products.[17,18] Although it would be attractive to substitute wastes for the costly feldspar when producing porcelain tiles, the complex densification mechanism limits the amount of waste that can be used when preparing dense tiles.[9,10,12]

These limitations could be changed by combining the production technology of porcelain and the properties of glass-ceramics, i.e. developing double-layer glass-ceramic/ceramic (porcelain) tiles. In contrast to the traditional glazing process, the double-layer tiles were formed by pressing two kinds of powders together. Furthermore, the glass-ceramic based on waste with good properties and aesthetical appearance can be selected as the top layer, while the substrate layer can incorporate a higher content of silicate waste without considering the influence of the impurity and densification resulting from the waste.

Bauxite tailings (BTs) are generated from a new process, the Bayer ore-dressing process[22] which uses medium- and low-grade bauxite ore to produce alumina in China. During the ore-dressing process, about 20 wt% ore goes into the waste. The major mineral compositions of BTs are: kaolinite (usually above 40 wt%), diaspore, illite and hematite; there are also small amounts of anatase, rutile and calcite.

In our previous work using BTs[23] and RM to prepare sintered glass-ceramics, the frits based on BTs were shown to exhibit good sintering ability, and the final product looked like a commercial tile. Frit from BTs was therefore used to prepare the glass-ceramic layer. However, the frit based on RM is brick red in color, although it has a composition similar to that of BTs, except for the TiO_2 content. It can be incorporated into the substrate layer.

* Corresponding author. Tel.: +86 371 67767671; fax: +86 371 67766629.
E-mail address: yanghz_74@yahoo.com.cn (H. Yang).

0955-2219/$ – see front matter © 2009 Elsevier Ltd. All rights reserved.
doi:10.1016/j.jeurceramsoc.2009.01.007

Table 1
Chemical compositions of RM and BTs (wt%).

Waste	SiO_2	CaO	Al_2O_3	Fe_2O_3	MgO	TiO_2	K_2O	Na_2O	LOI*
RM	12.33	17.24	29.89	8.08	1.57	4.80	0.24	8.12	17.73
BTs	25.27	6.05	37.19	10.66	0.15	3.89	3.06	0.99	12.74

* LOI (loss on ignition).

2. Experimental procedure

2.1. Raw materials

The BTs and RM came from Zhengzhou Research Institute, Aluminum Corporation of China Limited (CHALCO). The waste was wet milled in an alumina jar for 18 h and then screened through a 200 mesh (75 μm) sieve. Above 95 wt% of the waste could be screened through the sieve. The screened waste was dried at 120 °C for 24 h and then hammer milled.

Other raw industrial materials such as: quartz sand, sodium carbonate and lime came from Luoyang Float Glass Group Co. Ltd. These raw materials were also screened through 200 mesh (75 μm) sieves.

The chemical compositions of BTs and RM were determined by X-ray fluorescence and are given in Table 1.

Two glasses were prepared using BTs and RM as raw materials, respectively. Their compositions lie in the pseudowollastonite phase field of the Na_2O–CaO–Al_2O_3–SiO_2 quaternary system,[24] and the composition point is the same for both BTs and RM. The calculated batch compositions are given in Table 2. Batches weighing about 1 kg were mixed and melted in a glaze furnace at 1500 °C for 30 min, and then quenched in water to obtain glass frits. The as-received glass frits were milled below 200 mesh (75 μm), and named GC30 and GC40 for BTs and RM, respectively. Their chemical compositions are given in Table 3.

2.2. Specimen processing

The powder for the substrate layer (labeled P-BOT) was prepared by mixing BTs, GC40 and quartz sand in a weight ratio of 40:40:20, and adding 8 wt% water. The powder for the top glass-ceramic layer (labeled P-TOP) was prepared by mixing GC30 with the addition of 6 wt% polyvinyl alcohol (PVA) solution, and the concentration of the PVA solution was 2 wt%.

Cylindrical specimens with a diameter of 35 mm and a thickness of 6.5 mm were prepared by uniaxial pressing at 40 MPa. Two different pressing processes, single-loading and double-loading, were used to prepare the cylindrical specimens. In the single-load process, 10 g of P-BOT and 2.5 g of P-TOP were placed in the mould successively and pressed at one time. In the double-load process, 10 g of P-BOT was placed in the mould and pressed, and then 2.5 g of P-TOP was placed on top and pressed. Based on our previous work[23] we used 2.5 g of P-TOP, given the density of the sintered GC30 glass-ceramic (about 2.6 g/cm^3). Specimens were named P1 and P2 for the single-load and double-load processes, respectively, and specimens without a glass-ceramic layer were also prepared.

Table 2
Components of batches GC40 and GC30 (wt%).

Sample	GC40	GC30
RM	40.3	–
BTs	–	31.5
Quartz sand	30.2	27.1
Sodium carbonate	6.7	9.0
Lime	22.8	32.4

All the specimens were dried in an oven at 110 °C for 24 h. After drying, the double-layer specimens were about 6.5 mm thick, and the top glass-ceramic layer was about 1.5 mm thick. These dried specimens were then fired in an electric furnace at 930, 950, 970 and 1000 °C, respectively, for 60 min at the soaking temperature and at a heating rate of 8 °C/min. After sintering, the double-layer specimens were about 6 mm thick and the top glass-ceramic layer was 1 mm thick.

2.3. Characterization techniques

Phase identification was performed using X-ray diffractometry with CuKα radiation (XRD) (Philips X'PERT PRO, Almelo, The Netherland). The microstructure of the thermally treated specimens was observed on a polished surface using a scanning electron microscopy (SEM) (JEOL JSM-6700F, Japan) via secondary electron images (SEI) and backscattered electron images (BSI). Energy dispersive spectroscopy (EDS) (INCA 7421, England) was used to identify the local chemical composition. The crystallization process was investigated using differential scanning calorimetry (DSC) (SETARM Labsys, France) at a heating rate of 10 °C/min. The glass transition temperature (T_g), the onset crystallization temperature (T_{on}) and the peak crystallization temperature (T_p) were also determined by DSC experiments. The thermal expansion coefficients (TEC) were measured on bulk samples with dimensions of 5 mm × 5 mm × 50 mm on a dilatometer (model: RPZ-2A, China).

The mechanical strength of the fired specimens was evaluated using a three-point bending strength test on a universal testing machine (Zwick/Roell Z030, Germany) with a cross-head speed of 0.5 mm/min and a span of 30 mm. The fired specimens were cut to a cross-section of 4 mm × 5 mm. The double-layer specimens, P1 and P2, were polished to obtain thicknesses of about 0.5 mm for the glass-ceramic layer and 4.5 mm for the substrate layer, and were measured in the direction perpendicular to the layer alignment. The glass-ceramic layer was polished down to 0.5 mm to simulate the finish allowance in the final industrial polishing process.

Table 3
Chemical compositions of GC40, GC30 and the substrate (wt%).

Sample	SiO_2	CaO	Al_2O_3	Fe_2O_3	MgO	TiO_2	K_2O	Na_2O
GC40	44.04	24.66	14.90	4.04	0.78	2.40	0.12	9.01
GC30	45.11	25.26	15.31	4.39	0.06	1.60	1.26	7.02
Substrate	50.09	13.00	22.05	6.22	0.39	2.66	1.34	4.23

The linear shrinkage of a specimen was assessed to be the difference between the diameter of the dried specimen and that of the fired specimen divided by the diameter of the dried specimen. Water absorption and bulk density were measured using a device (model: XQK-02, China). The Vickers hardness of the top layer was measured on a micro-hardness tester (model: HVS-1000, China) with a load of 500 g and a dwell time of 10 s. Seven tests were conducted under identical conditions.

3. Results and discussion

The DSC curves of GC40 and GC30 are shown in Fig. 1. For GC40, T_g, T_{on} and T_p are 670, 827 and 993 °C, respectively, and $T_{on}-T_g$ is 157 °C. For GC30, T_g, T_{on} and T_p are 700, 880 and 975 °C, respectively, and $T_{on}-T_g$ is 180 °C. It should be noted that it is difficult to determine T_g (500 or 700 °C) from the DSC curve of GC30. A dilatometric analysis on glass fragments confirmed that the T_g of GC30 is about 700 °C. Similar thermal analysis curves have been seen elsewhere,[17] where the glass-ceramics were also developed from waste.

Generally, the Hrubÿ parameter, K_H, obtained by differential thermal analysis (DTA) or DSC, indicates the stability of the glass against crystallization on heating.[25] It is defined as

$$K_H = \frac{T_{on} - T_g}{T_m - T_{on}}, \quad (1)$$

where T_{on}, T_g and T_m are, respectively, the onset crystallization temperature (on heating), glass transition and melting temperatures estimated by DSC. According to Hrubÿ, the higher the value of K_H of a certain glass, the higher its stability against crystallization on heating. For a certain glass system, the value $T_{on}-T_g$ can approximately reflect its sintering ability. Twenty glasses with different compositions within the Na_2O–CaO–Al_2O_3–SiO_2 system were tested. These glasses with $T_{on}-T_g > 150$ °C exhibited good sintering ability (not shown here). As shown in Fig. 1, $T_{on}-T_g$ for GC40 and GC30 is 157 and 180 °C, respectively, and the sintering experiments are consistent with this.

According to the value of T_p for GC30 (975 °C), the experimental sintering temperature for the double-layer tile is in the range 930–1000 °C.

Fig. 2a and b shows, respectively, the XRD spectra of GC40 and GC30 fired at 1000 °C. From Fig. 2a, we can see that the crystal phases of fired GC40 are: gehlenite, wollastonite, albite calcian low and nepheline. Fig. 2b shows that the crystal phases

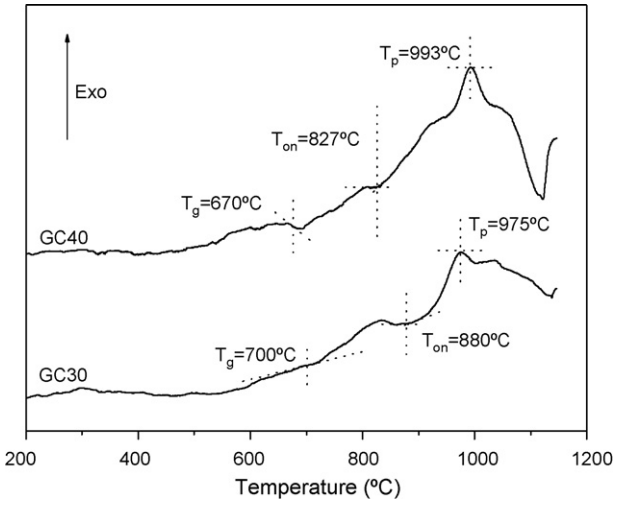

Fig. 1. DSC curves of GC40 and GC30.

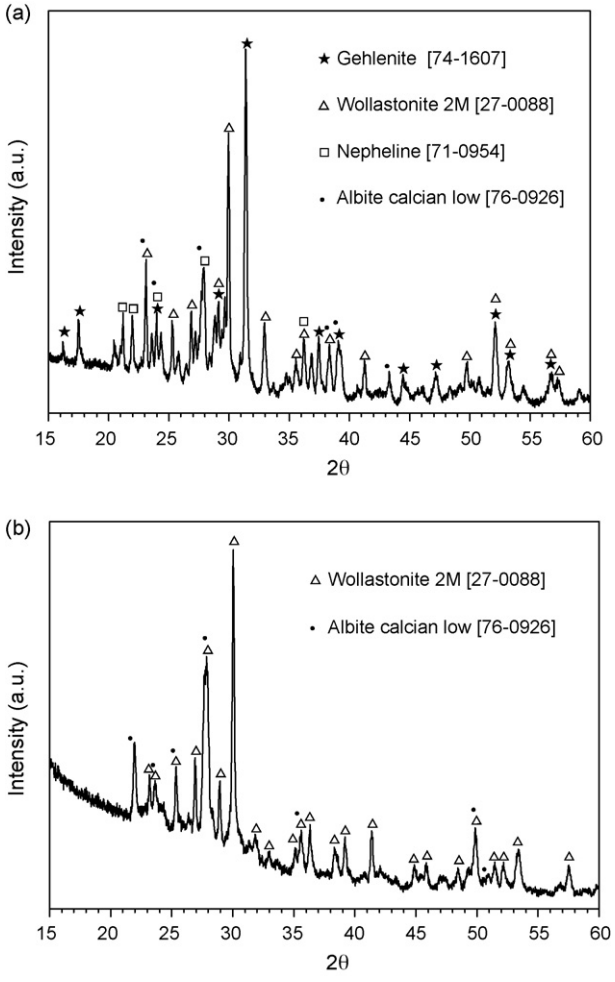

Fig. 2. XRD spectra of (a) GC40 and (b) GC30 fired at 1000 °C.

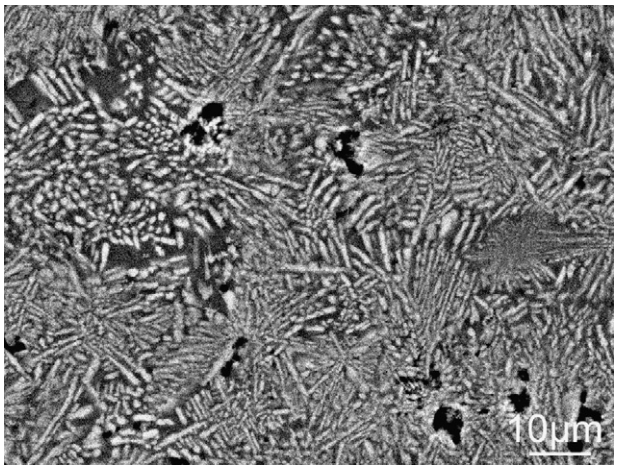

Fig. 3. SEM image of the polished surface of the glass-ceramic layer of P1 fired at 1000 °C.

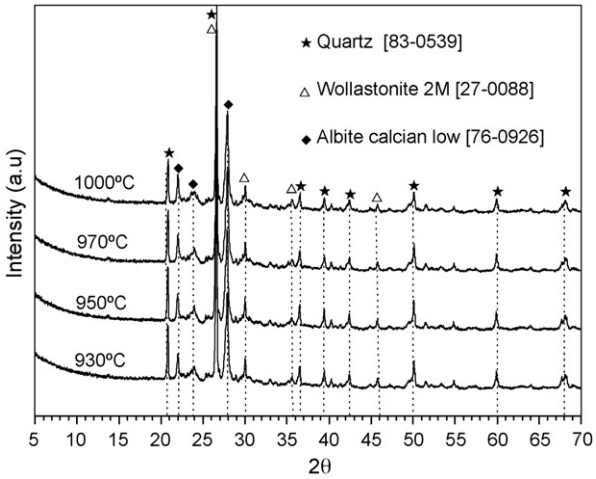

Fig. 5. XRD spectra of the substrate layer fired at 930–1000 °C.

of GC30 are wollastonite and albite calcian low, with wollastonite being the main crystal phase. The different crystal phases of GC40 and GC30 could be related to their different TiO_2 content. As shown in Table 3, for GC40, the content of TiO_2 is 2.40 wt%, while it is 1.60 wt% for GC30. DSC analyses on powders with different sizes confirm that both GC40 and GC30 have a surface crystallization mechanism.[26] Therefore, the higher TiO_2 content of GC40 cannot change its crystalline mechanism, but it results in different crystal phases in GC40. The different crystal phases of GC40 and GC30 could also be related to their different colors. GC40 is brick red in color, while GC30 is pale grey with more Fe_2O_3 content (Table 3). This could be explained by a different atomic environment for the iron in the structure of the crystal phases.[27]

The SEM image of the polished surface of the glass-ceramic layer (GC30) of P1 fired at 1000 °C is shown in Fig. 3. The glass-ceramic layer is well crystallized. The pale area is Ca-rich, corresponding to the wollastonite phase, which displays a needle-like granular morphology.

The DSC/TG curves of the substrate material are shown in Fig. 4. To simulate the firing specimens, the DSC sample was cut from the green body of the substrate. Two endothermic peaks and one exothermic peak were identified. The first endothermic peak at 75 °C is due to hygroscopic water. The second endothermic peak at 553 °C is due to the dehydroxylation of kaolinite with a weight loss of 2.66%. The third exothermic peak at 970 °C may be related to the metakaolinite decomposition to form other phases[28] and the crystallization of GC40 (see Fig. 1).

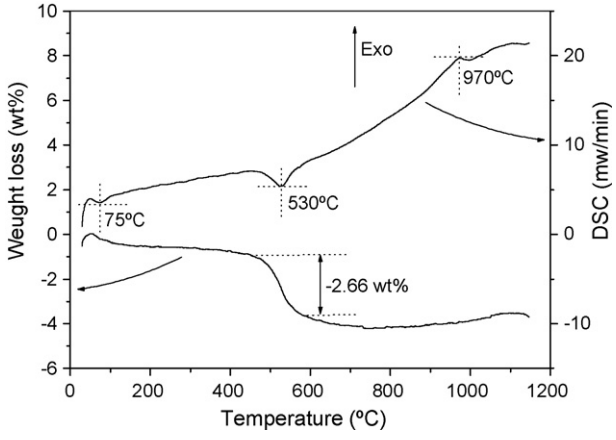

Fig. 4. DSC/TG curves of the substrate.

Fig. 5 shows the XRD spectra of the substrate layer fired at different temperatures. In the range 930–1000 °C, the crystalline phases of the substrate layer are quartz, wollastonite and albite calcian low. The presence of wollastonite and albite calcian low is due to the crystallization of GC40. It is interesting that gehlenite was not detected, which differs from the information in Fig. 2a, where gehlenite constituted the major crystal phase. This may be due to the possibility that GC40 could react with the aluminosilicate residues from the kaolinite decomposition and could cause the change in the surface composition of the GC40 particles, which is unfavorable to the formation of gehlenite.

The SEM images of the substrate layer fired at 930, 970 and 1000 °C are shown in Fig. 6a–f. The pale areas indicated by the arrows are GC40, and are Ca-rich. As seen in Fig. 6a–d, when fired at 930–970 °C, GC40 particles in the substrate layer are isolated, and this microstructure cannot enhance the densification of the substrate layer. Even when fired at 1000 °C, some of GC40 is connected (see Fig. 6e and f). No densification is observed due to the changed morphology of the GC40. The linear shrinkage of the substrate confirms this. When fired at 930–1000 °C, the linear shrinkage of the substrate has a constant value of 1.42%.

Although incorporating GC40 in the substrate formulation cannot enhance the densification of a substrate which has been fired at 930–1000 °C, it can increase its strength. For example, the specimen prepared under the same process as the substrate with BTs 100 wt% shows a bending strength of 22.83 ± 2.46 MPa when fired at 1000 °C. The bending strength of the substrate when fired at 1000 °C is 44.48 ± 2.74 MPa, which is about twice the former value. This characteristic is helpful when incorporating other vitrified wastes and waste glasses into the substrate formulation.

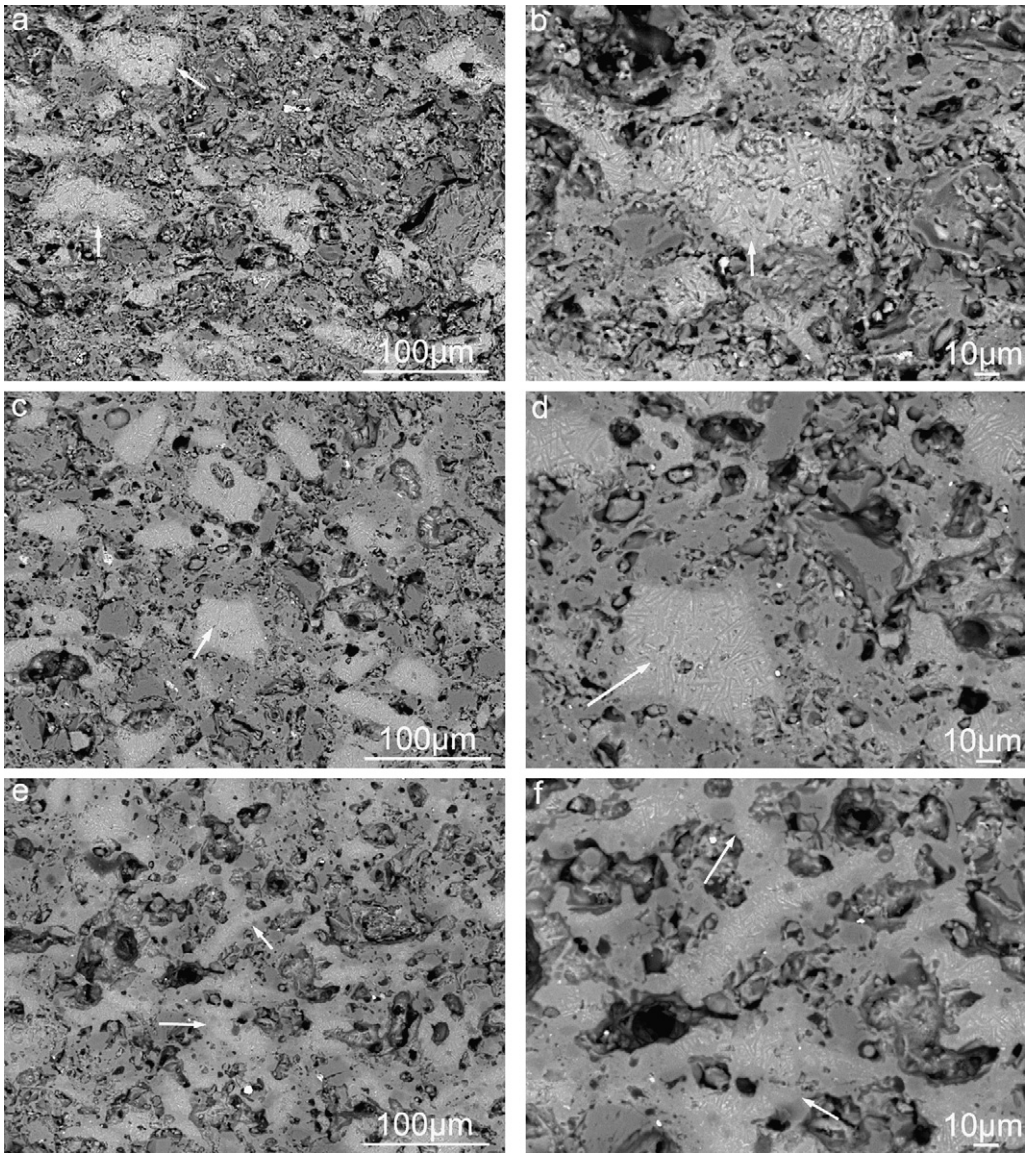

Fig. 6. SEM images of the substrate fired at 930 °C (a and b), 970 °C (c and d), and 1000 °C (e and f).

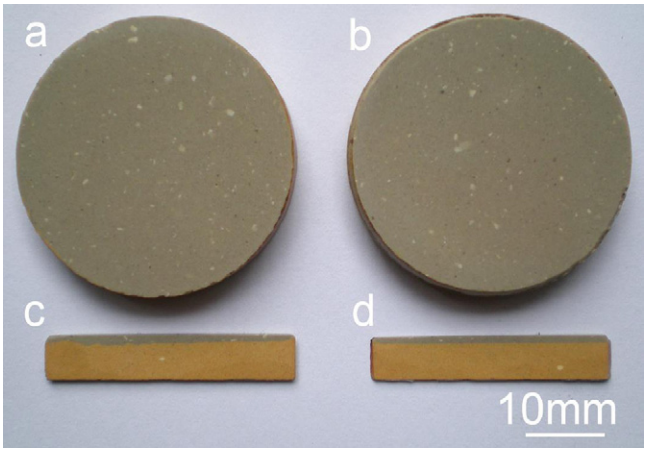

Fig. 7. Photographs of P1 (a and c) and P2 (b and d) fired at 1000 °C, (a and b) and (c and d) for the polished glass-ceramic surface and the polished cross-section surface, respectively.

Fig. 7a–d shows the photographs of P1 and P2 specimens fired at 1000 °C after polishing. Fig. 7a and b shows the polished surface of the glass-ceramic layer of P1 and P2, respectively. Fig. 7c and d shows the surface of the cross-sections. As shown in Fig. 7a and b, both P1 and P2 specimens have a satisfactory appearance. As shown in Fig. 7c, the thickness of the glass-ceramic layer of P1 is inhomogeneous, this is related to the preparation of the green body. In fact, the current industrial distributing device can ensure a thickness of 0.1 mm. The single-load process is appropriate for preparing the green body.

To examine the surface quality in detail, Fig. 8a–c shows the SEM images of the polished surfaces of a commercial porcelain tile and that of P1 and P2 fired at 1000 °C. For P1 and P2, the size of large pores is below 100 μm. As seen in Fig. 8a, the pores in the porcelain tile show clear boundaries. Some pores with irregular boundaries are related to the crystallization seen from Fig. 8b and c (indicated by an arrow).[29]

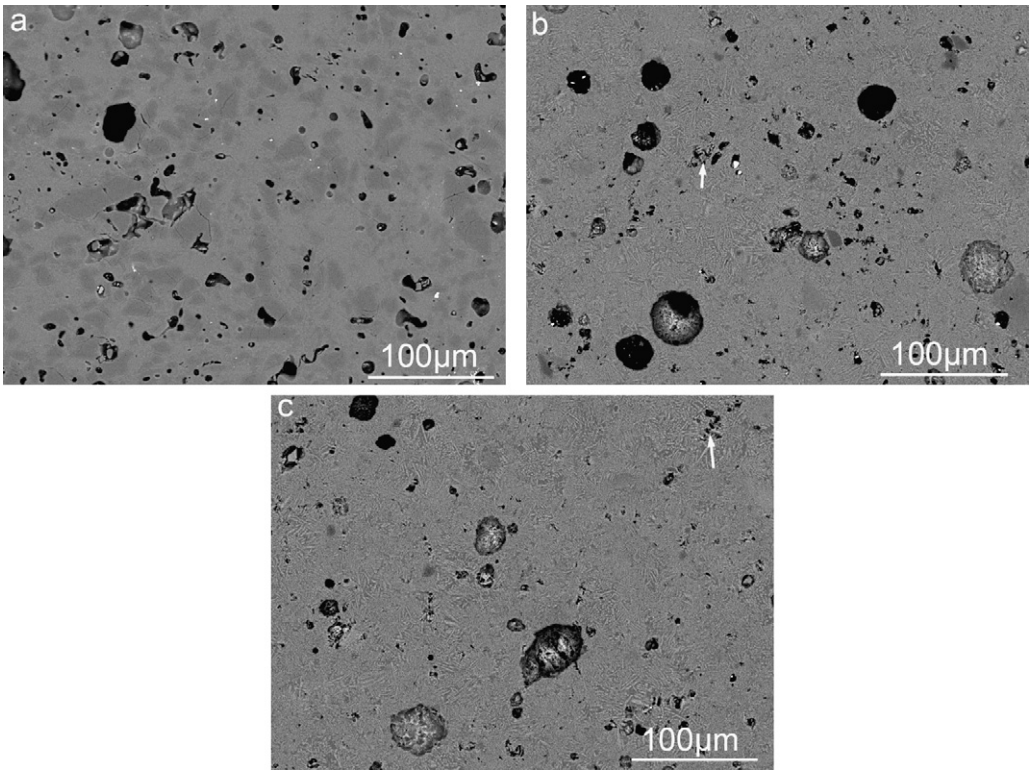

Fig. 8. SEM images of the polished surfaces of the samples: (a) a commercial porcelain stoneware; (b) P1 and (c) P2 fired at 1000 °C.

The SEM images of the polished cross-section surfaces of P1 and P2, fired at 1000 °C, are shown in Fig. 9a and b, respectively. The specimens show good bonding between the two layers. Interface defects, such as detaching or cracking, are not observed.

None of the fired P1 and P2 specimens suffer macro-deformation in the direction parallel to the layer alignment. This can be related to fact that the thermal expansion coefficients of the top layer and the bottom layer are very similar. The linear thermal expansion coefficient ($200\,^{\circ}C < T < 900\,^{\circ}C$) of GC30 (top layer) and the substrate are 8.13×10^{-6} and $8.29 \times 10^{-6}\,^{\circ}C^{-1}$, respectively.

The bending strength of the substrate, P1 and P2 (see Fig. 10), increases with the firing temperatures. Among them P1 and P2 show a bending strength higher than that of the substrate. When fired at 930–970 °C, the bending strength of P2 is higher than that of P1. It is interesting that when fired at 1000 °C, P1 and P2 have nearly same bending strength (about 51 MPa). The morphology of GC40 could influence the bending strength of the substrate. As shown in Fig. 6c–f, when fired at 1000 °C, some GC40 are connected and the bending strength of the substrate obviously increases. The strengths of P1 and P2 are reasonable due to the glass-ceramic layer, which has a bending strength about 80 MPa when fired at 930–1000 °C. In the bending strength tests, the glass-ceramic layer was about 0.5 mm in thickness, and the substrate was about 4.5 mm thick. Compared with P2, the different behavior of P1 could be related to the inhomogeneous thickness of the glass-ceramic layer and the change of interlayer. When fired at 930 °C, the bulk densities of P1 and P2 have the same value (2.22 g/cm^3), however, P1 has a lower bending strength.

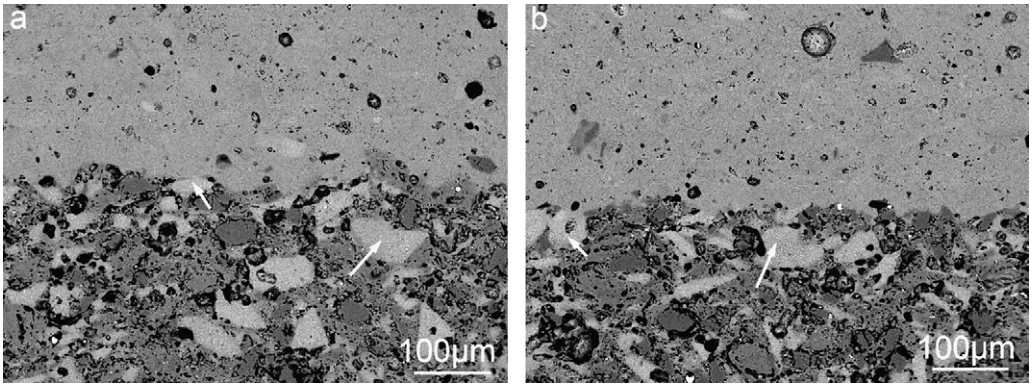

Fig. 9. SEM images of the polished cross-section surface of (a) P1 and (b) P2 fired at 1000 °C.

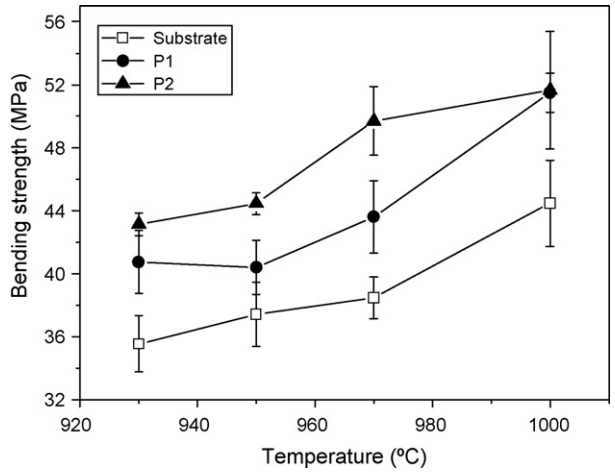

Fig. 10. Bending strength of the substrate, P1 and P2 fired at 930–1000 °C.

The fact that, when fired at 1000 °C, P1 and P2 exhibited the same bending strength could be related to the influence of the interlayer. EDS analysis shows that the thickness of the interlayer is about 5 μm for P1 fired at 1000 °C, while it is about 1 μm if fired at 930 °C. It should be noted that due to the similar compositions of GC30 and GC40, the thickness of the interlayer is determined by the contact areas, where the Ca-content is obviously different.

The Vickers hardness of the top layer of P1 fired at different temperatures is shown in Table 4. When fired at 930–1000 °C, the Vickers hardness changes within the range 5.86–6.63 GPa. The variation in Vickers hardness is related to the volume friction of the crystal phases and the microstructure. When fired at 930 and 950 °C, the Vickers hardness increases from 6.50 to 6.63 GPa. This can be attributed to the increase in the volume friction of the crystal phases. When fired at 970 °C (nearly equal to T_p), the Vickers hardness is 5.86 GPa due to the influence of the microstructure. At T_p, the crystal phase has the maximum growth rate, and this could result in a coarser microstructure. When fired at 1000 °C, the Vickers hardness increases to 6.32 Gpa. This is related to the change in microstructure. Therefore, as Mcmillan[30] stated, the maximum hardness approaches, but is not equal to, the value for the crystal phase due to the influence of the microstructure.

When fired at 930–1000 °C, the bulk density and water absorption of the substrate show a small variation of 2.13–2.14 g/cm^3 and 8.81–8.24%, respectively. Although the substrate layer has a higher water absorption, the double-layer tiles with integrated properties can be compared with porcelain tiles. Moreover, the sample sintered with a heating rate of 20 °C/min and holding time of 5 min at 1000 °C shows properties similar to those of a sample fired at 8 °C/min. Therefore, it is possible to sinter the double-layer tiles with a short sintering time, since fine glass powders are favorable to both sintering and surface crystallization.[31]

Table 4
Vickers hardness of the glass ceramic layer of P1 at 930–1000 °C.

Firing temperature (°C)	Hardness (GPa)
930	6.50 ± 1.04
950	6.63 ± 1.27
970	5.86 ± 0.55
1000	6.32 ± 0.45

4. Conclusions

This work has demonstrated the feasibility of preparing double-layer glass-ceramic/ceramic tiles from BTs and RM. The total amount of waste used in the specimens could reach 56% of their total weight (40% BTs plus RM in GC40). The top glass-ceramic layer shows a good bond with the substrate under a single-step sintering process. The glass-ceramic also shows good properties. This work should help in the production of high quality two-layer ceramic tiles and in recycling industrial waste.

References

[1]. Colombo, P., Brusatin, G., Bernardo, E. and Scarinci, G., Inertization and reuse of waste materials by vitrification and fabrication of glass-based products. *Curr. Opin. Solid State Mater. Sci.*, 2003, **7**, 225–239.
[2]. Bingham, P. A. and Hand, R. J., Vitrification of toxic wastes: a brief review. *Adv. Appl. Ceram.*, 2006, **105**, 21–31.
[3]. Rawlings, R. D., Wu, J. P. and Boccaccini, A. R., Glass-ceramics: their production from wastes—a review. *J. Mater. Sci.*, 2006, **41**, 733–761.
[4]. Souza, G. P., Rambaldi, E., Tucci, A., Esposito, L. and Lee, W. E., Microstructural variation in porcelain stoneware as a function of flux system. *J. Am. Ceram. Soc.*, 2004, **87**, 1959–1966.
[5]. Luz, P. and Ribeiro, S., Use of glass waste as a raw material in porcelain stoneware tile mixtures. *Ceram. Int.*, 2007, **33**, 761–765.
[6]. Raimondo, M., Zanelli, C., Matteucci, F., Guarini, G., Dondi, M. and Labrincha, J. A., Effect of waste glass (TV/PC cathodic tube and screen) on technological properties and sintering behaviour of porcelain stoneware tiles. *Ceram. Int.*, 2007, **33**, 615–623.
[7]. Rambaldi, E., Carty, W. M., Tucci, A. and Esposito, L., Using waste glass as a partial flux substitution and pyroplastic deformation of a porcelain stoneware tile body. *Ceram. Int.*, 2007, **33**, 727–733.
[8]. Karamanov, A., Karamanova, E., Ferrari, A. M., Ferrante, F. and Pelino, M., The effect of fired scrap addition on the sintering behaviour of hard porcelain. *Ceram. Int.*, 2006, **32**, 727–732.
[9]. Matteucci, F., Dondi, M. and Guarini, G., Effect of soda-lime glass on sintering and technological properties of porcelain stoneware tiles. *Ceram. Int.*, 2002, **28**, 873–880.
[10]. Tucci, A., Esposito, L., Rastelli, E., Palmonari, C. and Rambaldi, E., Use of soda-lime scrap-glass as a fluxing agent in a porcelain stoneware tile mix. *J. Eur. Ceram. Soc.*, 2004, **24**, 83–92.
[11]. Tarvornpanich, T., Souza, G. P. and Lee, W. E., Microstructural evolution on firing soda-lime-silica glass fluxed whitewares. *J. Am. Ceram. Soc.*, 2005, **88**, 1302–1308.
[12]. Andreola, F., Barbieri, L., Corradi, A., Lancellotti, I. and Manfredini, T., Utilisation of municipal incinerator grate slag for manufacturing porcelainized stoneware tiles manufacturing. *J. Eur. Ceram. Soc.*, 2002, **22**, 1457–1462.
[13]. Qian, G. R., Song, Y., Zhang, C. G., Xia, Y. Q., Zhang, H. H. and Chui, P. C., Diopside-based glass-ceramics from MSW fly ash and bottom ash. *Waste Manage.*, 2006, **26**, 1462–1467.
[14]. Wu, J. P., Rawlings, R. D., Boccaccini, A. R., Dlouhy, I. and Chlup, Z., Waste not, want not—an inexpensive glass-ceramic from waste. *Am. Ceram. Soc. Bull.*, 2006, **85**, 29–32.
[15]. Yoon, S. D. and Yun, Y. H., Waste glass and fly ash derived glass-ceramic. *J. Mater. Sci.*, 2006, **41**, 4315–4319.

[16]. Boccaccini, A. R., Han, W. X., Dimech, C. and Rawlings, R. D., Glass ceramics of high hardness and fracture toughness developed from steel fly ash. *Mater. Sci. Technol.*, 2006, **22**, 1148–1154.

[17]. Karamanov, A., Pisciella, P. and Pelino, M., The effect of Cr_2O_3 as a nucleating agent in iron-rich glass-ceramics. *J. Eur. Ceram. Soc.*, 1999, **19**, 2641–2645.

[18]. Karamanov, A., Pisciella, P., Cantalini, C., Pelino, M. and Jantzen, C. M., Influence of Fe^{3+}/Fe^{2+} ratio on the crystallization of iron-rich glasses made with industrial wastes. *J. Am. Ceram. Soc.*, 2000, **83**, 3153–3157.

[19]. Romero, M., Rawlings, R. D. and MaRincon, J., Development of a new glass-ceramic by means of controlled vitrification and crystallization of inorganic wastes from urban incineration. *J. Eur. Ceram. Soc.*, 1999, **19**, 2049–2058.

[20]. Bernardo, E., Andreola, F., Barbieri, L. and Lancellotti, I., Sintered glass-ceramics and glass-ceramic matrix composites from CRT panel glass. *J. Am. Ceram. Soc.*, 2005, **88**, 1886–1891.

[21]. Erol, M., Kucukbayrak, S., Ersoy-Mericboyu, A. and Ovecoglu, M. L., Crystallization behaviour of glasses produced from fly ash. *J. Eur. Ceram. Soc.*, 2001, **21**, 2835–2841.

[22]. Yu, C. M., Bauxite beneficiation—a new way to develop alumina industry. *Light Metals*, 2000, **9**, 3–6 (in Chinese).

[23]. Yang, H. Z., Chen, C. P., Sun, H. W., Lu, H. X. and Hu, X., Influence of heat treatment schedule on crystallization and microstructure of bauxite tailing glass-ceramics coated on tiles. *J. Mater. Process. Technol.*, 2008, **197**, 206–211.

[24]. Spivak, J., *J. Geol.*, 1944, **52**(1), 24–52.

[25]. Cabral, A. A., Cardoso, A. A. D. and Zanotto, E. D., Glass-forming ability versus stability of silicate glasses. I. Experimental test. *J. Non-Cryst. Solids*, 2003, **320**, 1–8.

[26]. Ray, C. S. and Day, D. E., Identifying internal and surface crystallization by differential thermal analysis for the glass-to-crystal transformations. *Thermochim. Acta*, 1996, **280–281**, 163–174.

[27]. Ferrari, S. and Gualtieri, A. F., The use of illitic clays in the production of stoneware tile ceramics. *Appl. Clay Sci.*, 2006, **32**(1–2), 73–81.

[28]. Iqbal, Y., Lee, W. E. and Grutzeck, M., Microstructural evolution in triaxial porcelain. *J. Am. Ceram. Soc.*, 2000, **83**, 3121.

[29]. Karamanov, A. and Pelino, M., Sinter-crystallisation in the diopside-albite system: part I. Formation of induced crystallisation porosity. *J. Eur. Ceram. Soc.*, 2006, **26**(13), 2511–2517.

[30]. McMillan, P. W., *Glass Ceramics* (*2nd ed.*). Academic Press, London, 1979, pp. 216–220.

[31]. Barsoum, M. W., *Fundamentals of Ceramics*. Mcgraw-Hill College Division, 1996, pp. 302–344.